April 1984

THE CHROMOSPHERES OF CLASSICAL CEPHEIDS. 11. HIGH-RESOLUTION PROFILES OF THE Mg II *h* AND *k* LINES

Edward G. Schmidt
University of Nebraska-Lincoln, eschmidt1@unl.edu

Sidney B. Parsons
Laboratory for Astrophysics and Solar Physics, NASA/Goddard Space Fllght Center; and McDonald Observatory, The Un~verslty of Texas at Austin

THE ASTROPHYSICAL JOURNAL, 279:202–214, 1984 April 1

THE CHROMOSPHERES OF CLASSICAL CEPHEIDS. II. HIGH-RESOLUTION PROFILES OF THE Mg II *h* AND *k* LINES

EDWARD G. SCHMIDT[1]
Department of Physics and Astronomy, University of Nebraska

AND

SIDNEY B. PARSONS[1,2]
Laboratory for Astrophysics and Solar Physics, NASA/Goddard Space Flight Center; and McDonald Observatory, The University of Texas at Austin

Received 1983 July 15; accepted 1983 September 13

ABSTRACT

High-resolution spectra have been obtained with the long-wavelength camera of the *International Ultraviolet Explorer* for five Cepheids at a number of phases each. These data were used to study the profiles of the Mg II *h* and *k* lines near 2900 Å. An emission feature often appears at the centers of the two lines. There are also central absorption features due to circumstellar or interstellar gas. They are often multiple and may or may not divide the emission into two peaks. The velocities of the circumstellar absorption components imply that they originate in a region which is at least several tenths of a stellar radius in extent. The strength of the emission rapidly increases to a maximum during rising light. It then tends to decline over most of the rest of the cycle, although there are instances of secondary maxima. The mean flux of the emission is lower than for nonvariable stars of similar temperature and luminosity, but at maximum strength the emission is appropriate to the instantaneous temperature.

Subject headings: stars: Cepheids — stars: chromospheres — ultraviolet: spectra

I. INTRODUCTION

The classical Cepheids occupy the region of the H-R diagram between nonvariable, luminous stars which are known to possess chromospheres and those for which chromospheres, if they exist, have not been found. For this reason and because we might expect to find that the chromospheres of Cepheids are affected by the pulsation of the stars, it is of interest to attempt to detect them and to study their properties.

The existence of chromospheres at some phases of some Cepheids and in many nonvariables was demonstrated with ground-based observations (Wilson and Bappu 1957; Kraft 1957) using the Ca II H and K emission cores. More recently, space-based telescopes have made it possible to study chromospheres in more detail because there are numerous ultraviolet emission features associated with the chromosphere. Several surveys of chromospheric activity in cool nonvariable stars have been published (e.g., Böhm-Vitense and Dettmann 1980; Ayres, Marstad, and Linsky 1981; Hartmann, Dupree, and Raymond 1982) in addition to more intensive studies of individual stars. In view of the particular interest in chromospheres of Cepheids, we undertook a program to study several of these stars with the *International Ultraviolet Explorer*. The first paper in this series (Schmidt and Parsons 1982, hereafter Paper I) discussed the results obtained at low resolution for five bright Cepheids, δ Cep (period = 5.4 days), η Aql (period = 7.2 days), β Dor (period = 9.8 days), ζ Gem (period = 10.2 days), and l Car (period = 35.5 days). The present paper continues this work by presenting high-resolution profiles of the Mg II *h* and *k* lines of the same stars. Preliminary Mg II emission-line strengths were illustrated and discussed by Böhm-Vitense, Parsons, and Schmidt (1982).

[1] Guest Observer at the *International Ultraviolet Explorer* observatory.
[2] Senior NRS-NASA Research Associate.

II. THE OBSERVATIONS

The observations presented in this paper were all obtained with the long-wavelength spectrograph of *IUE* in the high-resolution mode. In Table 1 the exposures are listed together with the Julian Dates and the phases of the stars at mid-exposure, the exposure times, and the spectrograph aperture used. The ephemerides used for the phases are the same as in Paper I. It can be seen that most of the spectra were taken through the large aperture of the spectrometer. However, it was originally thought that the resolution would suffer from the use of the large aperture so some of the earlier spectra were taken with the small aperture.

Several investigators have derived photometric calibrations for high-resolution *IUE* spectra. We have used the calibration of Cassatella, Ponz, and Selvelli (1981), which is based on a comparison of high-resolution spectra with low-resolution spectra. The low-resolution calibration is the same as used in Paper I. The large aperture of the spectrometer accepts nearly all of the light from a point source, and it is to spectra taken through that aperture that the calibration refers. The proportion of the starlight which goes through the small aperture differs appreciably from one exposure to another, so a general calibration applicable to the small aperture is not possible. To determine the calibration factor appropriate to the small-aperture spectra, we have integrated the flux over a 50 Å wide band centered at 2800 Å. The derived magnitude at 2800 Å, $m(2800)$, can then be compared with a known magnitude for

TABLE 1

LOG OF EXPOSURES

IUE Image No. LWR	JD 2,440,000+	Phase	Exposure Time (minutes)	Aperture
		δ Cephei		
3249	3866.33	0.822	60	S
3259	3866.84	0.916	35	S
3263	3867.28	0.998	20	S
5427	4108.23	0.899	30	L
5508	4120.91	0.261	40	S
6650	4252.21	0.729	35	L
6655	4252.51	0.785	48	L
6659	4252.78	0.837	30	L
6660	4252.82	0.844	32	L
9142	4538.44	0.069	13	L
9150	4538.86	0.148	35	S
9165	4540.46	0.445	35	L
9173	4540.99	0.543	40	L
9188	4542.64	0.851	34	L
9189	4542.68	0.860	32	L
9190	4542.73	0.868	30	L
9193	4542.87	0.894	25	L
9196	4543.04	0.926	32	S
		η Aquilae		
4943	4059.19	0.180	35	S
5506	4120.75	0.758	80	S
6263	4207.40	0.831	80	S
6265	4207.57	0.855	50	L
6267	4207.68	0.871	40	L
9144	4538.52	0.968	36	S
9149	4538.81	0.008	30	S
9153	4539.03	0.038	15	L
9156	4539.78	0.143	20	L
9162	4540.07	0.185	24	L
9166	4540.54	0.249	26	L
9172	4540.94	0.304	25	L
9191	4542.78	0.561	48	L
9200	4543.77	0.699	50	L
		β Doradus		
3231	3864.41	0.643	80	S
3244	3865.76	0.780	50	S
3252	3866.48	0.854	45	S
3257	3866.74	0.880	35	S
3265	3867.37	0.944	30	S
6268	4207.82	0.534	50	L
6652	4252.32	0.055	35	S
6657	4252.68	0.091	18	L
9152	4538.96	0.177	22	L
9167	4540.60	0.343	35	L
9194	4542.93	0.580	40	L
9202	4543.69	0.687	30	L
14164	5225.82	0.961	12	L
		ζ Geminorum		
5504	4120.60	0.000	35	S
5510	4121.09	0.049	35	S
6143	4192.76	0.109	12	L
6191	4196.97	0.523	52	L
6269	4207.89	0.599	40	L
9148	4538.72	0.186	30	L
9160	4539.97	0.310	35	L
9170	4540.80	0.392	48	L
9187	4542.58	0.567	40	L
9195	4542.99	0.607	36	L
9201	4543.90	0.697	30	L
14163	5225.66	0.866	25	L
		l Carinae		
6654	4252.44	0.891	32	L
9146	4538.62	0.943	35	L
9158	4539.87	0.978	25	L
9168	4540.68	0.001	27	L
9186	4542.45	0.051	30	L
9203	4544.04	0.096	32	L

that star at that particular phase to obtain the calibration factor. For two of the small-aperture spectra, LWR 5504 and LWR 6652, a value for $m(2800)$ was available from a low-resolution spectrum taken at the same time (Paper I). For the others the values of $m(2800)$ were obtained by interpolating to the appropriate phase in the light curve of the star. The light curves were formed using the magnitudes determined from both the low-resolution spectra in Paper I and the high-resolution spectra taken through the large aperture. It was found that the high-resolution magnitudes agreed well with those from Paper I when they occurred at nearly the same phase. Thus, the high-resolution spectra have been calibrated accurately to the same flux scale as was used for the low-resolution spectra.

III. THE LINE PROFILES

The profiles of the Mg II lines in solar-temperature stars are complex and composed of several components. The wide photospheric h and k absorption lines overlap, and the entire region is blanketed with numerous photospheric absorption lines of various elements. Any chromospheric emission component which is present is superposed on this complex background, from which it must be separated. Generally there is a narrow absorption feature which overlies the emission and which is attributed to circumstellar or interstellar material. In the case of the Cepheids this feature greatly complicates the appearance of the emission because the width of the absorption and its position relative to the emission vary with phase and from star to star. This suggests that part of the absorption is circumstellar and reacts to the pulsation of the star. However, considering the amount of reddening these stars suffer, we must also expect an interstellar component. In the following discussion we will refer to the central absorption as circumstellar and will leave the problem of separating any interstellar component to be considered in § IV.

In order to obtain the intensity of the emission lines without the contribution of the photosphere, it is necessary to estimate the shape of the photospheric component. We have done this by fitting a function of the form

$$F = F_c \exp\left[-\tau_h(\lambda) - \tau_k(\lambda)\right]$$

TABLE 2

PARAMETERS OF THE Mg II *h* AND *k* LINES

IMAGE NUMBER LWR	PHASE	EMISSION COMPONENTS λ2796 Type	F_e 10^{-12} (ergs cm^{-2} s^{-1})	V_e (km s^{-1})	W_e (Å)	S/L	EMISSION COMPONENTS λ2803 Type	F_e 10^{-12} (ergs cm^{-2} s^{-1})	V_e (km s^{-1})	W_e (Å)	S/L	CIRCUMSTELLAR ABSORPTION COMPONENTS Within Emission	Outside Emission	NOTES
δ Cephei:														
3249	0.822	B	0.80	+7	1.5	0.25	C	0.22	−88	0.5	...	−10, 39:	...	
3259	0.916	C	1.8	−64	0.7	...	C:	1.2	−54	0.5	...	−52, +44 (+17, +82)	...	
3263	0.998	A	...	...	...	...	A	...	...	...	...	+24 (−10, +33)	...	
5508	0.261	B	1.2	+28	2.8	0.86	A	...	...	...	...	−126, −105, −54, 2:	...	a
6650	0.729	C	0.35	−60	0.3	...	C	0.34	−45	0.3	...	−137, −71:, +2:, +92:	...	b
6655	0.785	B	0.50	−58	0.5	...	A	...	...	...	...	−2 (−34:, −14:, +3:, +21:, +36:)	−125, −83, +71:	b
6659	0.837	C	0.39	−73	0.5	...	C	0.24	−73	0.4	...	−67, +9 (−6, +27)	−137, −115, +75	a
6660	0.844	A	...	...	...	...	A	...	...	...	...	−75:, −5, (−15, +24)	−110	
9142	0.069	A	...	...	...	...	A	...	...	...	...	...	−66:, −25:, +23	
9150	0.148	B	1.9	+37	2.2	0.6:	A	...	...	...	...	+6	−115, −62:	a
9165	0.445	B	0.34	−2	1.6	0.6	A	...	...	...	...	+4	−115	
9173	0.543	B	0.84	−2	2.0	0.75	C?	0.32	−64	0.4	...	−100:, −68:, −10	...	
9188	0.851	B	2.3	−5	2.9	1.1	C	0.59	−75	0.9	...	−88:, −70:, +1 (−7, +31)	...	
9189	0.860	B	2.4	−19	3.3	1.2	A	0.47	−85	0.5	...	−134, 0 (−13, +30)	...	
9190	0.868	B	2.6	−33	2.6	1.4	C	0.39	−72	0.3	...	−96:, −11, +40, +90	...	
9193	0.894	C	1.5	−79	0.6	...	C	1.9	−73	0.6	...	−41:, +18 (−4, +18, +53)	...	
9196	0.926	C	1.9	−73	0.9	...	C	0.76	−71	0.3	...	+36 (−42:, −11:, +19:, +67)	...	a, b
η Aquilae:														
4943	0.180	C	0.37	+68	0.5	...	A	...	...	...	...	−92, −4, +58:	...	
5506	0.758	A	...	...	...	...	A	...	...	...	...	...	−122, −35	a
6263	0.831	C	0.61	−109	0.5	...	C	1.8	−109	0.2	...	−162, −15	...	a
6265	0.855	C	>1.8	<−88	>0.4	...	C	2.1	−103	0.8	...	−171:, −137:, −8 (−20, +33:)	...	c
6267	0.871	C	3.3	−86	0.9	...	C	4.1	−83	0.7	...	+4 (−4, +42)	121	
9144	0.968	B	4.6	+33	2.6	0.97	C	0.80	−86	0.3	...	+17 (−45, +13, +59:, +75:)	...	a
9149	0.008	B	6.0	+15	2.7	1.1	A	...	...	...	...	+10 (−2, +54), −40:	...	a
9153	0.038	B:	3.1	+59	2.7	0.50	A	...	...	...	...	−41:, +20 (+11, +55), +90	...	
9156	0.143	C	0.41	+60	0.3	...	A	...	...	...	...	−106, +6 (−2:, +9, +34), +58:, +79	...	a
9162	0.185	B	0.94	+20	1.3	0.38	A	...	...	...	...	−33, +5, +72	...	a
9166	0.249	C	0.93	+71	0.7	...	A	...	...	...	...	−56:, −30:, +4, +55, +74	...	
9172	0.304	C:	0.24:	+66	0.6:	...	C	0.20	+62	0.2	...	−50, +10	+110, +125	
9191	0.561	B	1.7	0	1.9	1.3	B	1.1	−14	1.6	1.8	−135, +1, +77:, +98	+146 (122, 145, 167)	
9200	0.699	B	0.56	+18	1.7	0.33	B:	0.15	−1	1.3	0.6:	−119, −80, −8 (−28, +15), +55:	+86:	

TABLE 2—*Continued*

Image Number LWR	Phase	Emission Components: λ2796 Type	λ2796 F_e 10^{-12} (ergs cm^{-2} s^{-1})	λ2796 V_e (km s^{-1})	λ2796 W_e (Å)	λ2796 S/L	λ2803 Type	λ2803 F_e 10^{-12} (ergs cm^{-2} s^{-1})	λ2803 V_e (km s^{-1})	λ2803 W_e (Å)	λ2803 S/L	Circumstellar Absorption Components: Within Emission	Outside Emission	Notes
β Doradus:														
3231.....	0.643	B	5.0	+1	1.8	0.19	B	5.4	−16	1.9	0.37	−37, +40:, +169:	...	[a]
3244.....	0.780	B	8.3	+36	2.0	0.28	B	8.0	+30	2.0	0.45	−2, +100:	+174:	[a]
3252.....	0.854	B	8.1	+48	2.1	0.15	B	6.7	+33	2.0	0.23	−4, +167	...	[a]
3257.....	0.880	B	<14.2	+46	2.0	0.12	B	8.7	+26	2.0	0.50	+3, +96, +155	...	[a]
3265.....	0.944	B	4.9	+42	2.0	0.18	B	2.5	+25	1.9	0.22	−5, +55:, +83:, +98	...	
6268.....	0.534	C	0.60	+54	0.8	...	C	0.44	+37	0.5	...	−35, +70, +106	...	
6652.....	0.055	B	2.6	+32	1.7	0.20	B	1.8	+24	2.0	0.16	−15, +70, +131, +164	...	[a]
6657.....	0.091	B:	3.1	+36:	1.6:	0.07	B:	2.1	+39:	1.9:	0.22	−63, −5, +79:, +147	...	
9152.....	0.177	B	3.3	+17:	1.1	0.12	B	2.1	+8:	1.8	0.30	−27 (−61, +2), +48, +94, +158	...	
9167.....	0.343	C	1.1	+68	0.44	...	C	0.78	+68	0.54	...	−8, +54:, +83:	−58:, +148	
9194.....	0.580	C	0.56	+34	0.42	...	C	1.0	+49	0.75	...	−39 (−54, −27), +60	−80, +128, +153	
9202.....	0.687	B	3.7	−10	1.1	0.14	B	4.3	−21	2.2	0.31	−119, −47 (−79, −23), +136	...	
14164.....	0.961	C	2.1	+76	0.5	...	C	1.3	+73	0.5	...	−1, +110	−57	
ζ Geminorum:														
5504.....	0.000	B	2.6	0	2.1	<0.62:	B	1.6	−3	2.0	1.22	−6, +79, +126	−128	[a]
5510.....	0.049	B	3.0	+8	2.1	<0.62:	B	3.5	−11	1.6	0.77	−133, 0, +86:, +121	...	[a]
6143.....	0.109	B	5.6	−20	1.9	2.6	B	4.1	−9	2.1	1.8	−140, −104:, +6, +71:	+127	
6191.....	0.523	B	0.55	−17	1.5	0.23	B:	0.82	−28	1.7	0.37:	−128, −35, +33:	−162, +115	
6269.....	0.599	B	1.4	−24	1.9	0.61	B	1.8	−28	1.9	0.62	−140, −32, +42:, +93:	+133	
9148.....	0.186	B	3.3	−27	2.0	0.95	B	2.5	−29	1.9	1.21	−138, −107:, −31, +42, +66:	+124:	
9160.....	0.310	B	1.4	+4	1.9	0.29	B	1.1	−3	1.7	0.79	−83:, −14 (−44:, −19:, +21), 64, +103	...	
9170.....	0.392	B	1.1	−1	2.0	0.31	C	0.60	+56	0.5	...	−108, −28 (−54, −14), +50, +80, +110:	−151, +143:	
9187.....	0.567	B	2.6	−17	2.0	0.48	B	1.5	−24	1.9	0.38	−143:, −36, +96:, +125	+139, +166	
9195.....	0.607	B	2.9	−16	2.2	0.47	B	2.5	−22	1.9	0.51	−137, −34, +43, +90:, +115	−166:, +139	
9201.....	0.697	B	8.1	−17	2.4	0.84	B	6.7	−22	2.2	0.99	−154:, −20, +58:, +122:	+154:	
14163.....	0.866	B	4.0	−6	2.2	0.74	B	2.7	−11	2.0	0.87	−128:, −17, +56, +126:	−158	
l Carinae:														
6654.....	0.891	B	6.5	−36	2.5	2.2	B	10.	−59	2.8	3.4	−216:, −165, −6, +58, +105:, +155	...	
9146.....	0.943	B	16.	−27	2.8	2.6	B	21.	−36	2.6	3.7	−223, +16, +54:, +120, +149	...	
9158.....	0.978	B	19.	−4	3.1	2.0	B	19.	−10	2.9	2.3	−216, +30, +118:	...	
9168.....	0.001	B	17.	−5	2.9	1.6	B	18.	−8	3.0	2.0	−209:, +16, +96	...	
9186.....	0.051	B	16.	+11	3.0	1.4	B	13.	+12	2.8	1.4	−74, +26, +120:	...	
9203.....	0.096	B	14.	+8	2.8	1.2	B	11.	+12	2.7	1.1	−76:, +14, +180:	...	

[a] Camera fiducial near line center for λ2796. Uncertain width and velocity.
[b] Asymmetric profile for λ2796 emission causes uncertainty in velocity.
[c] Data dropout at location of λ2796 emission feature. Values given are limits due to this.

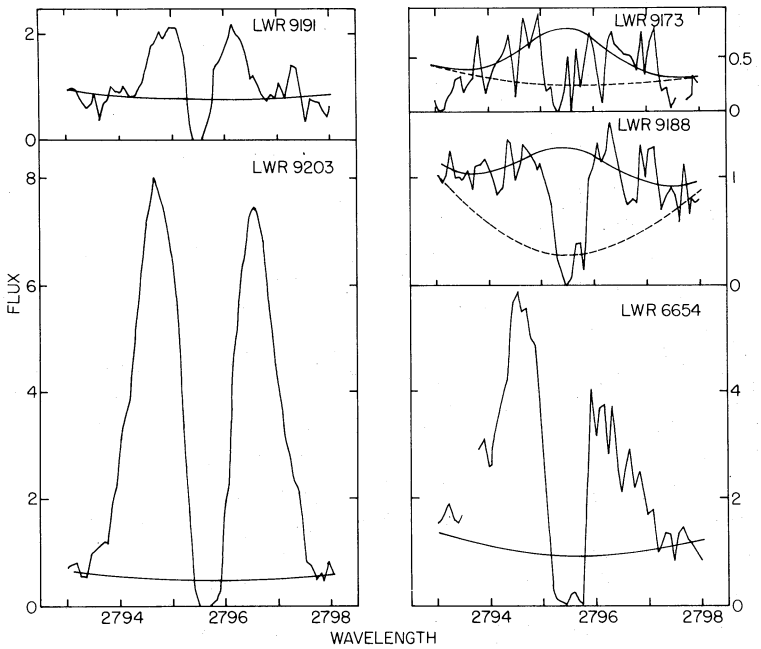

FIG. 1.—Examples of emission cores of type B. Each is labeled with the frame number, and all are for the λ2796 line. The various frames correspond to the various stars as follows: LWR 9191, η Aql at phase 0.56; LWR 9203, l Car at phase 0.10; LWR 9173, δ Cep at phase 0.54; LWR 9188, δ Cep at phase 0.85; LWR 6654, l Car at phase 0.89. The fitted photospheric absorption profile is shown as a smooth curve. A Gaussian profile which was fitted to the emission is also shown for LWR 9173 and LWR 9188. The gap in the profile from LWR 6654 near λ2793.5 is due to the presence of a camera fiducial. The flux is in units of 10^{-12} ergs s^{-1} cm^{-2} $Å^{-1}$, and the wavelength is in angstroms in all of the figures.

to the photospheric profile; F_c represents the continuum level, $\tau_k(\lambda)$ is the optical depth in the λ2796 line, and $\tau_h(\lambda)$ is the optical depth in the λ2803 line. Several forms were tried for the variation of the optical depth with wavelength, and it appeared that a Voigt function generally produced the best fits. It was therefore used for all the profiles. Since the oscillator strength for λ2796 is twice that for λ2803 (Wiese, Smith, and Miles 1969), we have assumed that $\tau_k(\lambda_0) = 2\tau_h(\lambda_0)$ and fitted to the observed photospheric profiles with F_c, the absorption coefficient of λ2796 at its central wavelength, and the damping parameter, in units of the Doppler width, as free parameters. The Doppler width was obtained from the microturbulent velocity. Experiments with different microturbulent velocities showed that the fit was insensitive to the value chosen, so it was simply taken from published spectroscopic analyses in the visible region (van Paradijs 1971; Schmidt 1971; Rodgers and Bell 1964, 1968). In fitting the profiles, we used the region from 2787 Å to 2810 Å but have excluded the part of the profile near the centers of the lines where the emission occurs and have excluded several small intervals with relatively strong absorption lines. Many weak absorption lines are, of course, included in the regions fitted. Since they are randomly distributed, they will have no systematic effect on the general shape of the Mg II absorption. The fitting is only intended to provide a baseline to use in extracting the emission-line strengths. Therefore, the success of this procedure should be assessed on the basis of whether it reproduces the photospheric line shapes adequately near the centers. The reader can judge this point from an examination of the line profiles shown in the various figures.

Table 2 contains measured parameters which characterize the Mg II cores. In examining the profiles it is obvious that the emission takes several distinct forms. In the third and eighth columns of the table there are letters which indicate the appearance of the profile. In some cases no emission can be seen above the noise level, and this is indicated by the letter *A*. Many of our spectra show double emission features separated by the circumstellar absorption component. Some examples are shown in Figure 1, and it can be seen that they are similar to what has been found in nonvariables of similar temperature (Stencel *et al.* 1980). Such profiles are indicated by the letter *B* in Table 2. Cases where the emission is only apparent on one side of the absorption are denoted by the letter *C*, and some examples are shown in Figure 2. The emission is to the longward side of the absorption in some cases and to the shortward side in others. These can be distinguished by referring to the velocities given in Table 2.

The strength of the emission component, F_e, is given in the fourth and ninth columns. It is the integrated flux above the fitted photospheric profile between the minima on either side of the emission line. Points which fell below the photospheric baseline (within the circumstellar absorption) were deleted. In Table 2 we also give the radial velocities of the emission, V_e. In setting the wavelength scale, the spectra were all shifted so that photospheric metal lines in this region had zero velocity. That is, the velocities in Table 2 are all relative to the photospheric lines. For the emission component, the meaning of the velocity depends on the form of the profile. For profiles with double emission features (type B), a Gaussian was fitted to the emission. The center of the Gaussian was taken to define the velocity. The resulting value represents the velocity of the emission with the circumstellar absorption

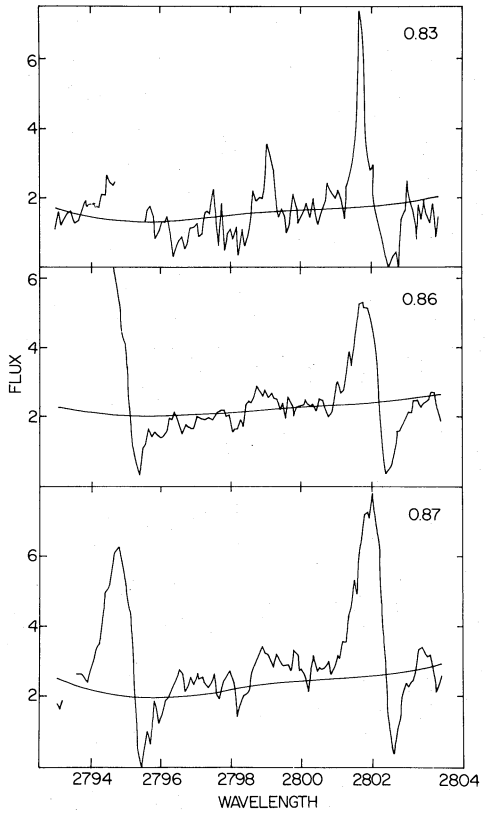

FIG. 2.—Examples of emission cores of type C. Both λ2796 and λ2803 are plotted. The frames shown are LWR 6263, LWR 6265, and LWR 6267, which are all spectra of η Aql during rising light. The spectra are labeled with phase and illustrate the increasing emission during this part of the star's cycle. The gap in the spectrum at phase 0.83 is due to a camera fiducial, while the short-wavelength region of the spectrum at phase 0.86 is missing because of a loss of data during transmission.

removed. For those cases in which the emission was only visible on one side of the absorption (type C), the velocity was measured at the center of gravity of the visible component. The actual velocity of the underlying emission will be nearer the photospheric velocity than the tabulated value. The sixth and eleventh columns list the width of the emission. For profiles of type B it was measured at an intensity of $0.5\langle I\rangle$, where $\langle I\rangle$ is the mean of the peaks of the two emission components. For type C emission the width is measured at half-maximum for the visible component. The seventh and twelfth columns of Table 2 give the intensity ratio between the shortward and the longward component of emission when both are present (type B).

The velocities of the various circumstellar absorption components relative to the photosphere are listed in the thirteenth and fourteenth columns of Table 2. The absorption is often multiple or appears to be composed of a number of overlapping components which are only partially resolved. When there appear to be well-separated absorption lines, the velocities are listed separately. When a broad feature appears to be composed of partially separated components, the mean velocity of the entire feature is given followed by estimates for the individual components in parentheses. The velocity of the main absorption feature is underlined. Again, the velocities are relative to the photosphere. In the table, we have separated components which are superposed on an emission from those which are outside any emission which may be present.

The identification of various features as Mg II absorption components presents serious difficulties. This can be appreciated by referring to the sample profiles shown in Figures 3–6. At times features are weak compared with noise. Because of the presence of a fiducial or the superposition of the steep edge of an emission component, a suspected absorption feature may only be visible in one member of the Mg II doublet. Photospheric lines and circumstellar lines of other elements are an additional source of confusion. That the latter are a possible problem is indicated by the fact that the asymmetry of Mg k emission in α Ori is due to circumstellar absorption by Mn I and Fe I (Bernat and Lambert 1976). However, since we have both the h and the k line and since we have multiple spectra at relatively close spacing in phase, it is possible to detect many spurious features and reject them. We first compared the profiles of h and k and recorded those absorption features which were obviously present in both. When a significant feature was present in one line but fell in a location in the other where it would be obscured by a fiducial or by the edge of an emission, it was recorded as uncertain and is marked with a colon in Table 2. The features on the preliminary list were further examined to eliminate any which were doubious. This included checking for coincidences with known photospheric lines from the solar spectrum, looking for components which did not appear on other spectra at nearby phases of the same star, and checking that all features which were accepted were significant compared with the noise in at least one line. Any which were found to be uncertain were deleted. Finally, the velocities of all components were plotted against phase. Absorption features which are actually circumstellar should not closely follow the photospheric velocity curve. Several which did were deleted as probable photospheric lines. In Table 2 we have separated the absorption features which are superposed on emission from those which are not because the latter are less certain. While these checks may have eliminated some real Mg II absorption features, they should ensure that most of those remaining are real.

If we assume that the circumstellar component of λ2796 should have the same velocity as that of λ2803, we can estimate the uncertainties of the velocities. We find that for δ Cep a single velocity has a standard deviation of 11 km s^{-1}, while it is 4 km s^{-1} for the other stars. The larger uncertainty for δ Cep is due to the inclusion of a number of noisy spectra and spectra with little or no emission against which to measure the absorption.

IV. THE CIRCUMSTELLAR ABSORPTION

In order to correct our velocities for the motion of the photosphere, we have used radial velocity curves from the following sources: Wallerstein (1979) for δ Cep; Jacobsen and Wallerstein (1981) for η Agl; Bell and Rodgers (1967) for β Dor; Jacobsen and Wallerstein (1982) for ζ Gem; Rodgers and Bell (1968) for l Car. The absorption-line velocity data are displayed in Figure 7 for four of the stars. Because of meager phase coverage, data for l Car are not plotted. The photospheric velocity curves are shown as solid lines, and the various components identified in the Mg II cores are shown

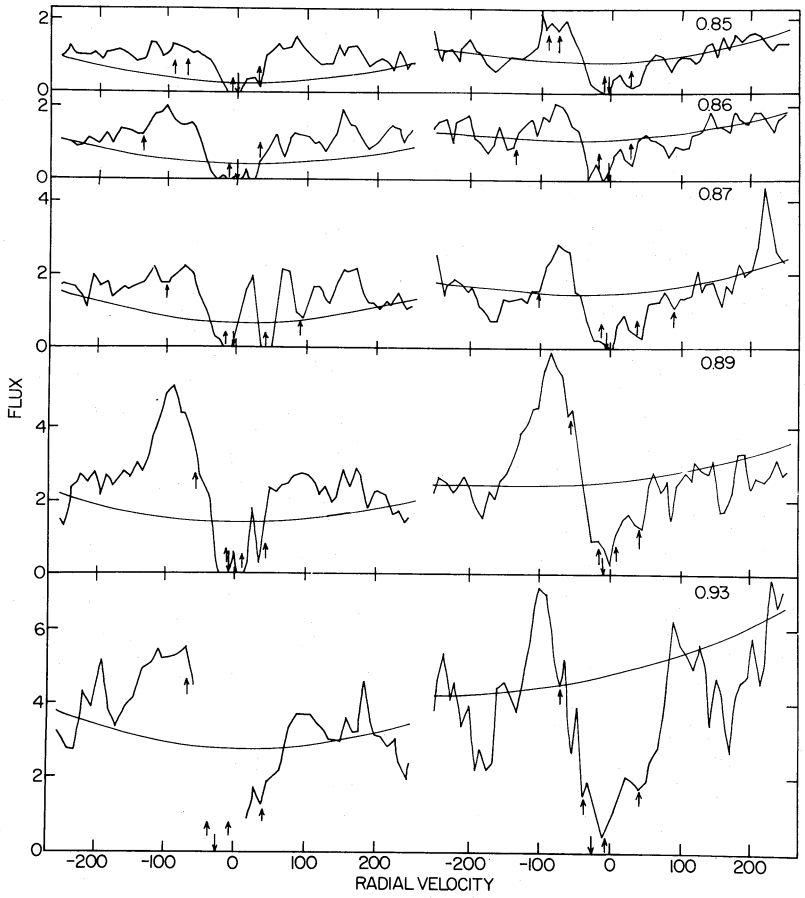

FIG. 3.—Profiles of the absorption cores of the Mg II lines in δ Cep. The profile of λ2796 is on the left, while the profile of λ2803 is on the right. Each is labeled with the phase, and the fitted photospheric profile is shown. The abscissa is labeled in units of heliocentric velocity relative to the rest velocity of each line. The photospheric velocity is indicated by a downward-pointing arrow on the axis. Upward arrows indicate the velocities from Table 2. Regions of the profile near fiducials have not been plotted. The spectra shown are LWR 9188, LWR 9189, LWR 9190, LWR 9193, and LWR 9196.

as circles. When multiple components were apparent, all have been plotted. Points which are indicated as uncertain in Table 2 are shown in Figure 7 by open circles, as are points representing features falling outside the emission. Individual open circles should be regarded with caution, and their reality can only be established by noting whether they fit into general trends. The main component (underlined in Table 2) is marked by a bar through the point. When the main component is a partial blend, and it is not obvious which of its components is dominant, all are marked.

A cursory inspection of Figure 7 shows that the various stars behave in different ways. However, for all of them the main component is nearly stationary in velocity throughout the cycle. In Table 3 we give the mean velocities of the photospheric velocity curves and of the main Mg II absorption component. Note that the scatter of the velocities of the stationary component (fourth column of Table 3) is significantly larger than the errors quoted in the previous section in most cases. Furthermore, the stationary component has a velocity which differs from the center-of-mass velocity of the star by up to 25 km s^{-1}. It is likely that this component is composed of an interstellar feature blended with stellar features. The latter should change velocity with phase, shifting the center of gravity of the line and increasing the scatter. There are several cases where an examination of the phase behavior of the line clearly shows that blended stellar features are causing shifts in the location. The difference between the stellar velocity and that of the stationary component is most likely explained by the presence of the interstellar component.

Examples of the shapes of the cores of the Mg II lines for δ Cep are shown in Figure 3. The flux is plotted against the heliocentric radial velocity relative to the rest wavelength of

TABLE 3

MEAN VELOCITIES

	⟨V⟩			
STAR	Photosphere	Stationary Circumstellar Absorption	σ FOR ONE POINT	STANDARD ERROR OF THE MEAN
δ Cep.....	−16	−9	8	2
η Aql	−15	−20	8	2
β Dor	+9	−3	7	2
ζ Gem.....	+8	−10	5	2
l Car	+1	+4	8	3

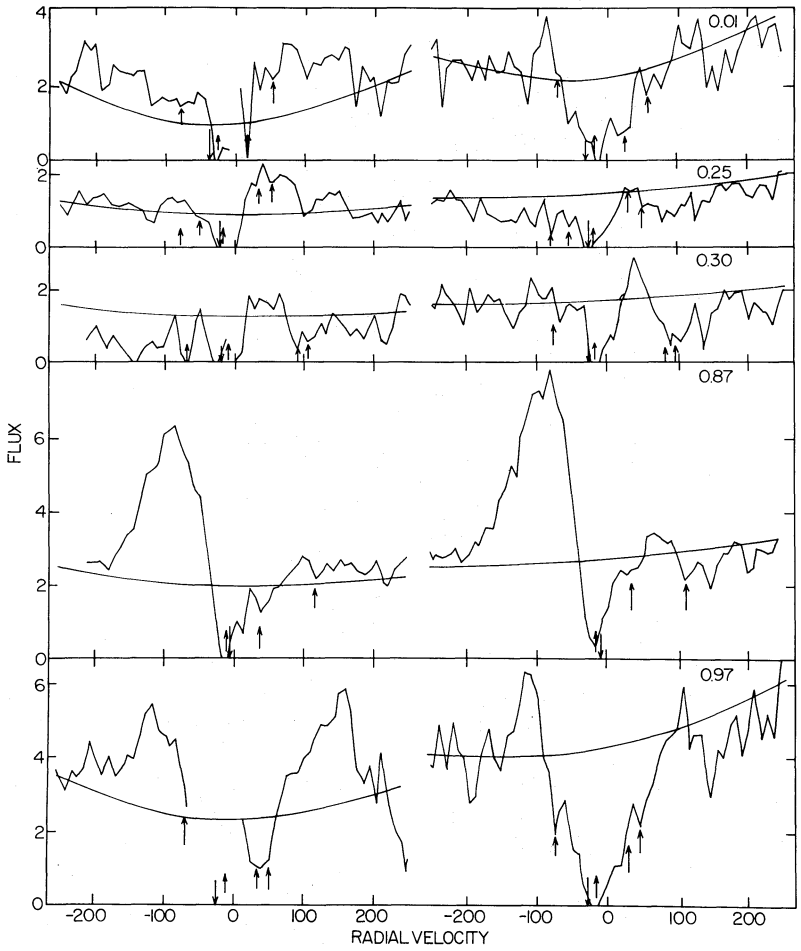

FIG. 4.—Profiles of the absorption cores of the Mg II lines in η Aql. These diagrams are plotted in the same way as in Fig. 3. The spectra shown are LWR 9153, LWR 9166, LWR 9172, LWR 6267, and LWR 9144 from top to bottom.

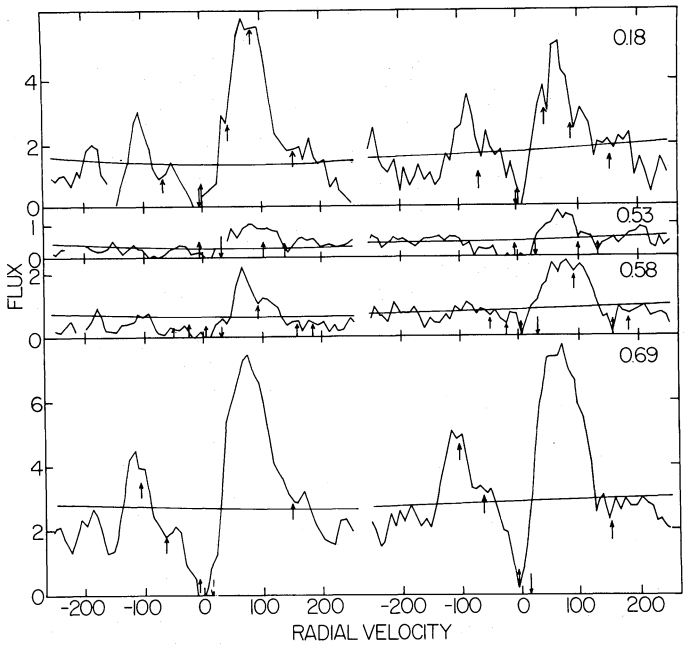

FIG. 5.—Profiles of the absorption cores of the Mg II lines in β Dor. The comments in the legend to Fig. 3 concerning the notation also apply to this diagram. The spectra shown are LWR 9152, LWR 6268, LWR 9194, and LWR 9202 from top to bottom.

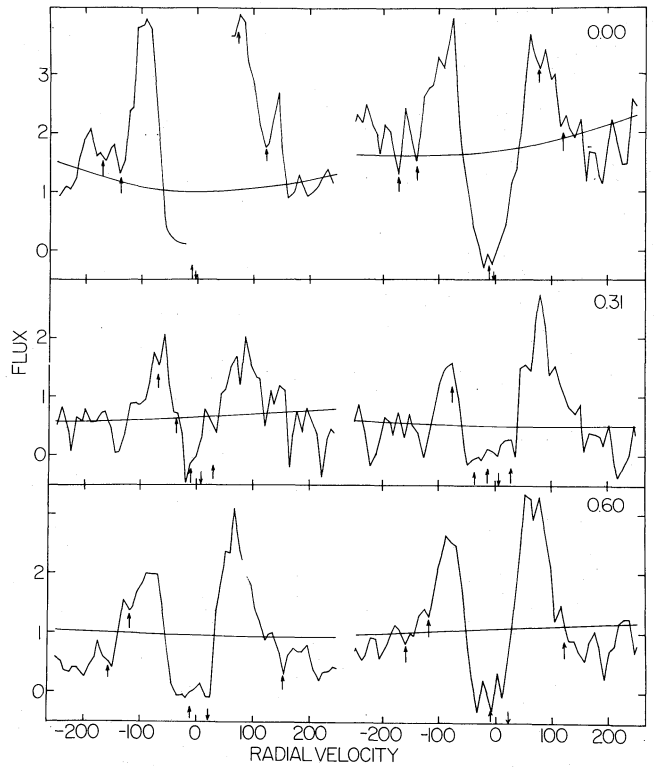

FIG. 6.—Profiles of the absorption cores of the Mg II lines in ζ Gem. This figure is plotted in the same way as Figure 4. The spectra illustrated are LWR 5504, LWR 6269, and LWR 9160.

the line, and the photospheric velocity is indicated by a downward-pointing arrow. The velocities of the absorption components in Table 2 are indicated by upward-pointing arrows. The spectra shown were obtained during rising light and show the development of the line as maximum light approaches. In every case a component is apparent to the right of the main absorption component. This appears in Figure 7 as the positive velocity (i.e., falling inward toward the star) component at velocities near $+30$ km s^{-1} which begins near phase 0.79 and persists for about 0.15 cycles. It can be seen that as maximum light is approached, this component increases in velocity and moves away from both the photospheric velocity and the main minimum of the line. This behavior indicates that it has been correctly identified as a component of Mg II, and that it overlies the photosphere and the chromosphere (since it is seen superposed on the emission feature in some cases, as at phase 0.85). Hα shows a similar behavior but with smaller velocity (Wallerstein 1979). The component at velocities near $+80$ km s^{-1} at these same phases is less certain and should be verified with further observations before it is regarded as established.

There are also negative velocity (i.e., rising from the star) components in Mg II visible much of the time. As can be seen in Figure 3, these are generally less certain than the positive velocity components. However, they are present on enough spectra and in a consistent enough fashion to indicate their reality. Although they present a complex appearance, it is possible to discern some possible trends with phase. The dashed lines were drawn by eye to follow one possible variation of the velocity. They represent a single line which goes through 1.9 cycles in a continuous manner although there is a decrease in the slope in the middle of the range. When the velocity is less than 80 km s^{-1}, the line corresponds to a deceleration of 12 cm s^{-2}. This is equal to the gravity at a distance of $\sim$1.4 stellar radii above the photosphere, while the surface gravity of the star is about 70 cm s^{-2} (using the mass and radius from Cox 1980). During the time this component is visible (nearly two cycles), it should rise a distance of more than two stellar radii. While it is unlikely that the same material is responsible for the absorption during such a long interval, these numbers give a rough indication of what is happening.

Turning now to η Aql, examples of line profiles at various phases are shown in Figure 4. As in δ Cep there are infalling components, but in this case they are present most of the time. The many components and the gaps in the phase coverage make it difficult to trace particular features through the cycle. The behavior does not resemble that of Hα (Jacobsen and Wallerstein 1981) as nearly as it did for δ Cep. Outward moving (negative velocity) components are also present most of the time. It is possible that these components show some outward acceleration or that some of them are constant in velocity. However, a definite conclusion is difficult. In the spectra in Figure 4 the component at about -55 km s^{-1} is visible at phases 0.04, 0.25, 0.30, and 0.97, but it was not deemed present at a measurable level in the spectra at phase 0.87. However, it can be seen that such a feature would fall on the sharp edge of the emission, and its presence cannot be ruled out. That this feature is a genuine component of the Mg II absorption is indicated by the fact that in some spectra (such as those at phases 0.04 and 0.97 in Fig. 4) it is within the emission component and therefore is located above the emitting region. We thus conclude that there is material moving away from η Aql with velocities greater than 50 km s^{-1} at least during part of the cycle. If this material persists at these velocities for times of the order of 0.3 cycles, it will move a distance of about a quarter of the stellar radius.

In the case of β Dor there are also multiple components during most of the cycle. At most phases the absorption has components at velocities of between -60 and -100 km s^{-1} relative to the photosphere. In Figure 5 the cores of Mg II in some spectra of β Dor are shown, and the displaced components are evident in several cases. Although it is not obvious in every spectrum whether they are due to Mg II, at several phases (such as 0.18 and 0.69 in Fig. 5) they are clearly within the emission feature and therefore due to overlying absorption. There are also longward-displaced components evident in both Figures 5 and 7. Again, we have drawn lines through these components to illustrate how they might exhibit continuity through the cycle. In this case we have marked three components which seem to persist over significant intervals of time. The slopes of these lines correspond to accelerations of between 5 and 11 cm s^{-2}. This is to be compared with the stellar gravity, which is about 37 cm s^{-2} at the photosphere. During the time they appear to persist, these components represent motions of the order of 0.9–1.6 stellar radii.

It can be seen in Figure 7 that ζ Gem exhibits absorption features with both positive and negative displacements. Some examples of the line core are shown in Figure 6, and it can be seen that the breadth of the central absorption is such that it might be composed of multiple components which are not

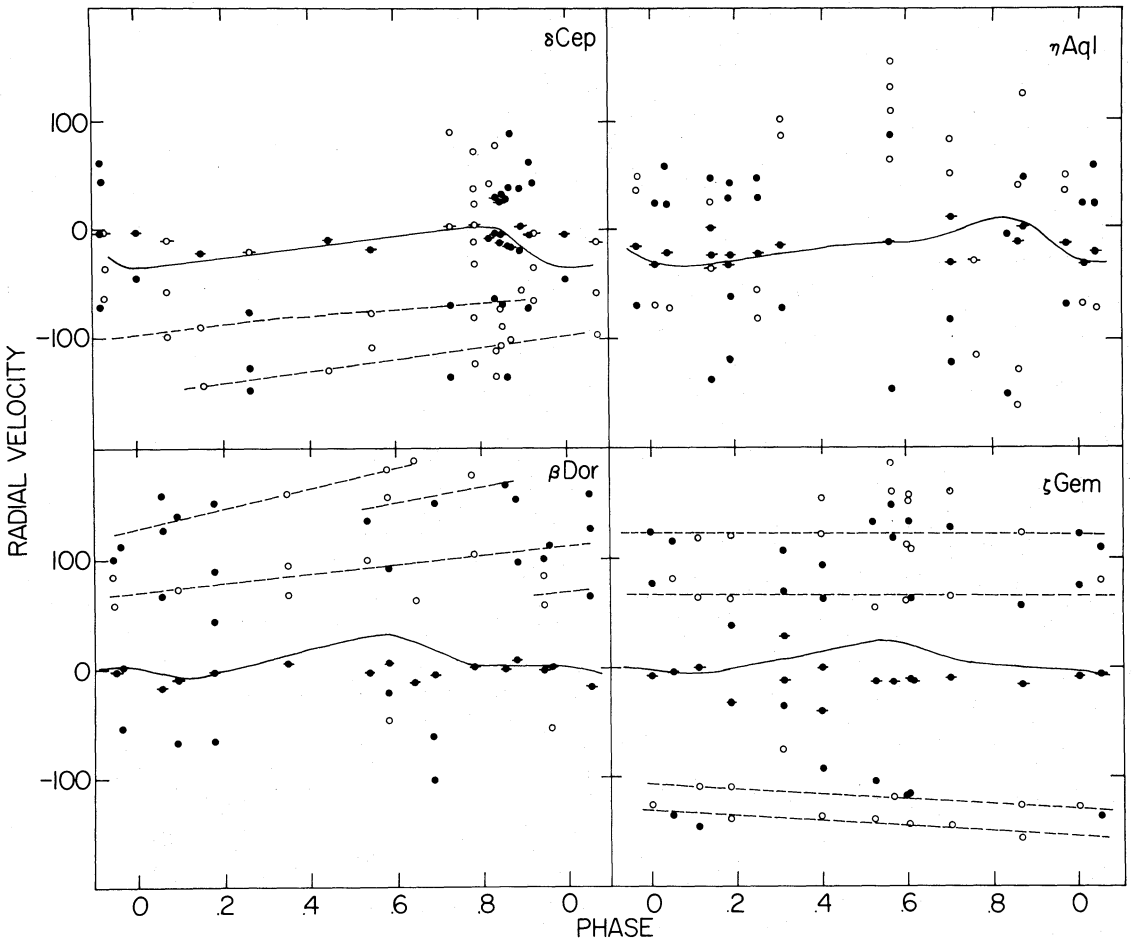

FIG. 7.—The velocities of the absorption components plotted against the phase for four Cepheids. The solid curves are the photospheric velocity curves, while the circles are the velocities of the absorption components of Mg II. Open circles denote points of lower weight. Circles with a bar through them represent the main line components. Dashed lines are eye fits to the points for the purposes of illustration and discussion. The velocities are in km s^{-1}.

well resolved. If any are present at the velocities observed by Jacobsen and Wallerstein (1982) for Hα, they will be lost in this central feature. The positively displaced components present a complex picture, and it appears possible that some of them are nearly constant in velocity, as indicated by the dashed lines. For the negative components there is some possibility of continuity for velocities larger than 100 km s^{-1}, as indicated by the dashed line. In that case the acceleration represented by the line is 1.3 cm s^{-2}, and if the component persists over 1.8 cycles as indicated, it will move a distance of about 4.4 stellar radii.

For l Car our phase coverage is so limited that we cannot study the behavior of the line with phase. In appearance the profiles resemble those of ζ Gem. The longward-displaced components are the most persistent and are seen on all our spectra. In particular, there appears to be a component at about 110 km s^{-1} most of the time. A component with a large negative velocity, −210 km s^{-1} is also present on most of our spectra. In this star the emission is so wide that this absorption is still within it and is therefore a secure identification. As in the other stars, these components imply large motions of the material even over the small interval of phase we have observed.

The interpretation of these velocities is uncertain because of a lack of models for chromospheres in these circumstances. However, there are some conclusions which can be drawn about the regions in which these features originate. It is obvious from looking at the variations of velocity with phase and the profiles that the behavior varies strongly among the stars and depends to some extent on period. In fact, a comparison of Figure 3 with Figure 5 shows that the appearance of the profiles has reversed between δ Cep and β Dor. How much of this behavior is related to the dynamics of the gas and how much is the result of excitation conditions is not certain.

Although the accelerations we mentioned above for the various features are not likely to represent actual motions of the material, we should not expect very much higher acceleration because they would exceed the gravitation of the star. Unless there is an unrecognized force on the gas, this is unlikely, particularly in the direction toward the star. With accelerations of that order, the observed velocities cannot be achieved in less than several tenths of a cycle. Therefore, they imply that elements of gas are accelerated for at least that long. This in turn implies that these elements move distances of the order of several tenths of the stellar radii, and the regions involved

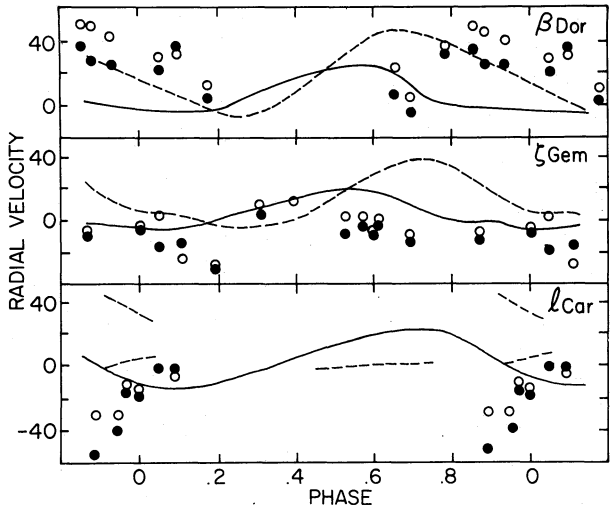

FIG. 8.—Velocities of the emission lines for these Cepheids. The solid curves represent the photospheric velocity, while the dashed lines are the velocities of the core of Hα. Open circles are the velocities of the Mg II λ2796 emission, while the fitted circles are those from Mg II λ2803.

are that large. In Cepheids the amplitude of the photospheric motion during the cycle is of the order of 10% of the radius. In order for elements of gas to avoid reacting directly with the pulsational motions, they must be significantly higher than that. The fact that some Mg II absorption components move differently from the photosphere thus supports the view that they originate at least several tenths of a stellar radius above it.

The chromosphere of the Sun is a few percent of the solar radius in depth. On the other hand, evidence exists (Stencel 1981) which indicates that red giants have chromospheres that extend to a number of stellar radii. The Cepheids appear to fall between these extremes.

Since there are both rising and falling elements which travel tenths of stellar radii, it is reasonable to suppose that the chromosphere is heterogeneous over the stellar surface and is likely composed of a number of rising and falling columns. This picture also fits with the facts that there are a number of components to the line at times and that tracing the velocity behavior with phase is difficult. By analogy with the Sun we might imagine that the chromosphere is composed of loops with rising and falling regions.

V. THE EMISSION LINES

In Figure 8 we have plotted the variation of the velocities of the emission lines for these stars at all phases for which both a longward and a shortward emission component were present (type B). The objects δ Cep and η Aql are not shown because the emission in these stars is very weak, and consequently the velocities are poorly determined. The open circles represent the velocities of λ2796, while the filled circles represent the velocities for λ2803. The velocity of the core of Hα is also shown as a dashed line. These data come from the same references which were cited for the photospheric radial velocity curves in the previous section. It is obvious that a systematic difference exists between λ2796 and λ2803 when both are present. In nearly every case the velocity for λ2803 is smaller than that for λ2796. The mean difference is 9 km s^{-1}. Since the oscillator strengths of the two lines are a factor of 2 different, they will form at somewhat different levels, and the effect we are seeing may be indicative of a different mean velocity at different levels. Another possibility is that the circumstellar components have different effects on the line profiles. Note that both lines have a mean velocity which obviously differs from the mean of the photospheric curve at least for β Dor and ζ Gem. This is also true of the core of Hα.

It can be seen that β Dor and ζ Gem behave rather differently in Figure 8. For β Dor the Mg II velocities seem to lag after the photospheric curve and show a larger amplitude. In this regard they are similar to the motions inferred from Hα except that the lag is larger. In ζ Gem, on the other hand, the velocity of the Mg II is generally more negative than that of the photosphere and does not resemble the Hα curve. It appears that the velocity slowly declines during most of the cycle but suddenly increases near phase 0.25. In the case of l Car the velocity of the Mg II emission increases over the interval of phase we have observed. It is reasonable to suspect that it might go through a maximum early in the cycle and thus resembles β Dor in behavior. It should be remembered, of course, that the velocity may not refer to the same elements of gas throughout the cycle. In fact, it is quite possible that the emission is composed of multiple elements, and that fitting a Gaussian to them as a whole is not valid. Thus, it is not clear how much of the behavior we see is due to dynamic effects and how much to changes in the gas being observed.

We have plotted the total flux of h and k in Figure 9 as a function of phase. The scale on the left side of the figure gives

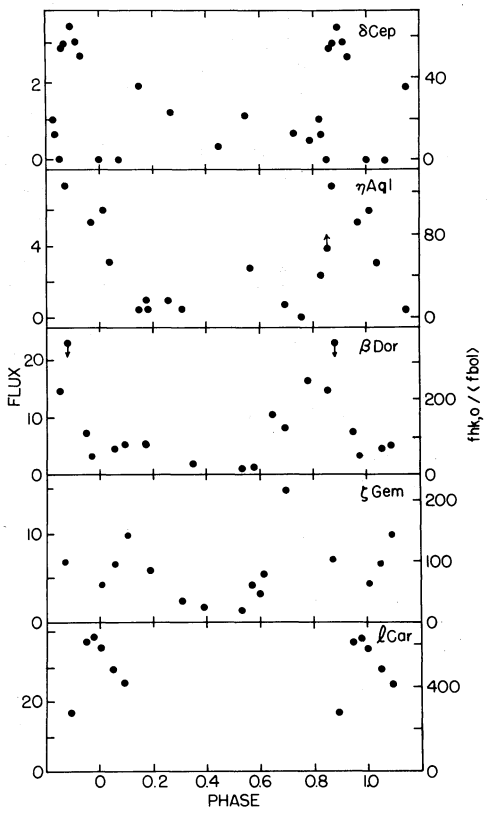

FIG. 9.—Integrated fluxes of the emission lines. The total flux of h and k is plotted as a function of the phase of the star. The scale to the left gives the flux observed at the Earth, while the scale to the right gives the flux in units of 10^{-7} times the bolometric flux. The latter has been corrected for interstellar absorption.

TABLE 4

PARAMETERS OF EMISSION FEATURES

Star	Phase of Rise of Emission		Phase of Bump on UV Light Curve	$\frac{\langle f_{\text{Mg II}}\rangle_0}{\langle f_{\text{bol}}\rangle_0}$	$\frac{f_{\text{Mg, max, 0}}}{\langle f_{\text{bol}}\rangle_0}$
	O I	Mg II			
δ Cep	...	0.82–0.90	0.75:	22×10^{-7}	65×10^{-7}
η Aql	...	0.8–0.87	0.7:	37×10^{-7}	125×10^{-7}
β Dor.....	0.7–0.8	0.6–0.8	0.65	100×10^{-7}	267×10^{-7}
ζ Gem	0.7–0.9:	0.56–0.7	0.7	83×10^{-7}	216×10^{-7}
l Car	0.9–1.0	0.84–0.94	...	243×10^{-7}	625×10^{-7}

the line flux at the Earth, while on the right we have placed a scale which gives the radiative losses in the Mg II lines in units of the stellar bolometric luminosity. The mean luminosity over the cycle was used, and corrections for interstellar absorption were made using the color excesses of Dean, Warren, and Cousins (1978) and the mean interstellar absorption curve of Savage and Mathis (1979). In Table 4 we have collected some parameters of the emission for reference.

As was the case for the other emission lines (Paper I), the Mg II appears to turn on rather suddenly and then decline during most of the cycle. However, there are possibly secondary peaks in several instances. In δ Cep the decrease near maximum light is probably not real since the lines are wide and difficult to separate reliably from the background profile. To determine the reality of features in the plot for δ Cep, it would be necessary both to obtain higher signal-to-noise data and to employ a more detailed and realistic scheme for determining the photospheric profile. In the case of η Aql the same considerations apply, but for ζ Gem the emission is stronger so that the background is of little significance. Therefore, the secondary rise in the emission after maximum light in ζ Gem is likely to be real. This was not seen in the other emission lines because of their weakness. It thus appears that Cepheid chromospheres are excited more than once during the cycle.

In Table 4 we have listed the phase of the main increase in the strength of the O I and Mg II emissions. Because of the lack of detailed phase coverage, the exact times of the beginning and the end of the increases are uncertain. However, it is clear from the data in Table 4 that the Mg II emission rises sooner than that of O I by about 0.1 cycles. The λ1305 O I line is excited by fluorescence from Lyβ and thus reflects the conditions where Lyβ forms. This is at somewhat hotter temperatures than the level of formation of Mg II so it is not surprising that it is excited slightly later in the cycle. As discussed in Paper I, there are apparent bumps on the far-ultraviolet light curves which occur at phases near the start of the chromospheric emission. In Table 4 we have listed the approximate phases at which these begin. Again, the phase coverage is such that we cannot give accurate values, but it can be seen that the bumps in the light curves occur at about the time of the start of the Mg II emission. This further strengthens our suggestion that the ultraviolet bump is an indicator of the passage of the same disturbance which gives rise to the chromospheric excitation.

In order to compare the Cepheids with nonvariable stars of similar temperature and luminosity, we have calculated the mean emission-line fluxes over the cycles. In the case of ζ Gem there is poor phase coverage, which could easily miss the time of the maximum strength of the Mg II emission. We have assumed that the point at phase 0.70 is the maximum of the emission, and that it decays smoothly until 0.17 cycles later, when we have another measurement. For l Car we have likewise assumed a smooth decay of the emission from our last point at phase 0.1 to zero at about phase 0.8. While these assumptions are not accurate, they will allow us to estimate how these stars compare with others. The resulting mean normalized fluxes and the maximum normalized fluxes are tabulated in Table 4.

In Figure 10 we have compared the Cepheids with nonvariable stars (data from Stencel *et al.* 1980; Ayres, Marstad,

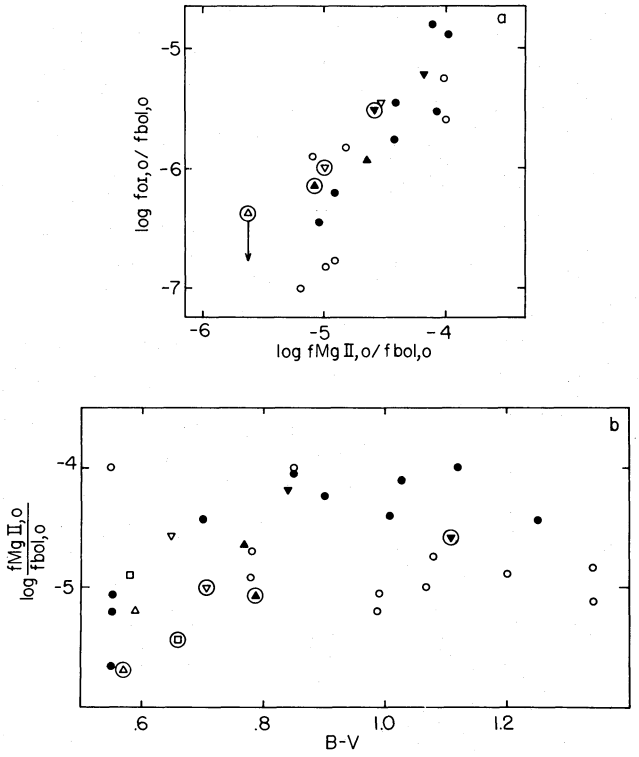

FIG. 10.—Comparison of the chromospheric emission of the Cepheids with that of nonvariable stars. The symbols denote the various stars as follows: *filled circles*, luminosity class I nonvariable stars; *open circles*, luminosity class II nonvariable stars; *open triangles with vertex up*, δ Cep; *squares*, η Aql; *open triangles with vertex down*, β Dor; *filled triangles with vertex up*, ζ Gem; *filled triangles with vertex down*, l Car. Circled symbols for the Cepheids denote means over the cycle, while symbols without circles are from the phase of maximum Mg II emission. Fig. 10*a* is a plot of the flux of λ1305 O I against the flux of Mg II $h + k$. Fig. 10*b* is a plot of the strength of Mg II $h + k$ against the intrinsic color.

and Linsky 1981; Simon, Linsky, and Stencel 1982). The published data have been corrected for interstellar absorption in the same way as was done for the Cepheids. In Figure 10*a* the flux of λ1305 O I (from Paper I for the Cepheids) is plotted against the flux of the Mg II emission. It can be seen that the Cepheids tend to fall above the nonvariables in this diagram; the O I emission is stronger at a given Mg II flux by a factor of 2–3 than would be the case with the nonvariable class I stars. This is in spite of the fact that in Paper I we found that the O I emission was generally weaker than in nonvariable stars. In Figure 10*b* the Mg II normalized flux is plotted against the intrinsic color. It can be seen that the luminosity class I stars generally show stronger surface fluxes than the class II stars by a factor of about 6. The Cepheids are luminous enough to be classed as Ib and should therefore resemble the more luminous stars in this diagram. In fact, their mean fluxes fall closer to the class II stars than to the class I stars. On the other hand, the line fluxes at the time of strongest emission fall quite near the few supergiants of similar color. Thus, it appears that when the emission is strongest, it is appropriate to the temperature of the star but at other times during the cycle the emission is weak for the temperature compared with nonvariable stars.

VI. DISCUSSION

One of the basic questions we raised at the start of this work was what effect the stellar pulsation has on the chromospheres. The fact that there are differences between the chromospheres of the Cepheids and the nonvariables as exemplified in Figure 10 and in Figure 7 of Paper I indicates that there is an effect. Since the chromosphere is weak on the average compared with nonvariables, we conclude that during much of the cycle, the pulsation acts to inhibit the formation of the chromosphere which would be appropriate to the instantaneous temperature and luminosity. At the phase of maximum Mg II emission, the chromosphere seems to be similar to the nonvariables. This occurs at the same phases when the microturbulence in Cepheids tends to increase above its usual value (see Evans 1980, for example). Unfortunately, an examination of the published spectroscopic studies of these five stars shows that the available data are insufficient for a detailed comparison of the time of the increase in microturbulence and the appearance of the chromospheric emission. These are also phases of maximum outward acceleration according to the radial velocity curves. Shocks occurring at that time might excite the chromosphere. Therefore, we are not able to determine whether the increased chromospheric acitivity we find during rising light is the result of increased convection or whether it arises from the appearance in the chromosphere of a shock generated by the pulsation. Further theoretical studies will be needed to resolve this question.

We are grateful to the staff of the *International Ultraviolet Explorer* observatory for the use of their facilities and their assistance in obtaining the observations described in this paper. S. B. P. held a National Research Council–National Aeronautics and Space Administration Senior Research Associateship during much of this work. This work was supported by the National Aeronautics and Space Administration under grants NSG 5328, NSG 5391, and NAG 5-282.

REFERENCES

Ayres, T. R., Marstad, N. C., and Linsky, J. L. 1981, *Ap. J.*, **247**, 545.
Bell, R. A., and Rodgers, A. W. 1967, *M.N.R.A.S.*, **135**, 124.
Bernat, A. P., and Lambert, D. L. 1976, *Ap. J.*, **204**, 830.
Böhm-Vitense, E., and Dettmann, T. 1980, *Ap. J.*, **236**, 560.
Böhm-Vitense, E., Parsons, S. B., and Schmidt, E. G. 1982, in *Pulsation in Classical and Cataclysmic Variable Stars*, ed. J. P. Cox and C. S. Hansen (Boulder: JILA), p. 238.
Cassatella, A., Ponz, D., and Selvelli, P. L. 1981, *NASA IUE Newsletter*, **14**, 170.
Cox, A. N. 1980, *Ann. Rev. Astr. Ap.*, **18**, 15.
Dean, J. F., Warren, P. R., and Cousins, A. W. J. 1978, *M.N.R.A.S.*, **183**, 569.
Evans, N. R. 1980, in *Current Problems in Stellar Pulsation Instabilities*, ed. O. Fischel, J. R. Lesh, and W. M. Sparks (NASA Tech. Memo. 80625), p. 237.
Hartmann, L., Dupree, A. K., and Raymond, J. D. 1982, *Ap. J.*, **252**, 214.
Jacobsen, T. S., and Wallerstein, G. 1981, *Pub. A.S.P.*, **93**, 481.
———. 1982, *Pub. A.S.P.*, **94**, 471.
Kraft, R. P. 1957, *Ap. J.*, **125**, 336.
Rodgers, A. W., and Bell, R. 1964, *M.N.R.A.S.*, **128**, 365.
———. 1968, *M.N.R.A.S.*, **138**, 23.
Savage, B. O., and Mathis, J. S. 1979, *Ann. Rev. Astr. Ap.*, **17**, 73.
Schmidt, E. G. 1971, *Ap. J.*, **170**, 109.
Schmidt, E. G., and Parsons, S. B. 1982, *Ap. J. Suppl.*, **48**, 185 (Paper I).
Simon, T., Linsky, J. L., and Stencel, R. E. 1982, *Ap. J.*, **257**, 225.
Stencel, R. E. 1981, in *Second Cambridge Workshop on Cool Stars, Stellar Systems and the Sun*, ed. M. S. Giampapa and L. Golub (*Smithsonian Ap. Obs. Spec. Rept.* No. 392).
Stencel, R. E., Mullan, D. J., Linsky, J. L., Basri, G. S., and Worden, S. P. 1980, *Ap. J. Suppl.*, **44**, 383.
van Paradijs, J. A. 1971, *Astr. Ap.*, **11**, 299.
Wallerstein, G. 1979, *Pub. A.S.P.*, **91**, 772.
Wiese, W. L., Smith, M. W., and Miles, B. M. 1969, NSRDS–NBS, Vol. 22.
Wilson, O. C., and Bappu, M. K. V. 1957, *Ap. J.*, **125**, 661.

S. B. PARSONS: Space Telescope Science Institute, Homewood Campus, Baltimore, MD 21218

E. G. SCHMIDT: Department of Physics and Astronomy, University of Nebraska, Lincoln, NE 68588